




Penalty coupling of trimmed isogeometric Kirchhoff–Love shell patches

Davide Proserpio¹ and Josef Kiendl ^{1,*}

¹Institute of Engineering Mechanics and Structural Analysis—Bundeswehr University Munich, Werner-Heisenberg-Weg 39, 85577 Neubiberg, Germany

*Corresponding author: josef.kiendl@unibw.de

ABSTRACT

We present a formulation for isogeometric Kirchhoff–Love shell analysis on complex CAD models consisting of multiple trimmed patches. The method is based on the penalty coupling method presented in Herrema AJ, Johnson EL, Proserpio D, Wu MCH, Kiendl J, Hsu MC (Penalty coupling of non-matching isogeometric Kirchhoff–Love shell patches with application to composite wind turbine blades. *Computer Methods in Applied Mechanics and Engineering* 2019;346:810–840.) and extended to the application on arbitrary coupling curves defined either in the physical or parametric space. We present the detailed formulation ready for implementation. Different numerical tests demonstrate the accuracy and applicability of the method.

KEYWORDS: isogeometric, Kirchhoff–Love shells, trimming, patch coupling

1. INTRODUCTION

Isogeometric analysis (IGA) has been introduced in [2], as a new paradigm to better link and eventually merge computer-aided design (CAD) and finite element analysis (FEA) through a unified geometry description. More precisely, the concept of IGA is to adopt the geometry description from CAD for analysis. The standard technology for geometry description in CAD is non-uniform rational B-splines (NURBS), and, consequently, NURBS have been adopted as shape functions for describing the geometry and approximating the solution in IGA. Besides their power in geometric modeling, NURBS have proven to be excellent shape functions for various kinds of analysis [3], and IGA has gained a lot of interest in many areas of computational mechanics. An area where IGA probably had the most impact is shell analysis, and many new shell element formulations have been developed making use of the specific properties of NURBS as shape functions [4–14]. This holds especially for element formulations based on the classical Kirchhoff–Love shell theory, where the smoothness of NURBS finally enabled the formulation of simple element formulations satisfying the necessary C^1 continuity inherent to the theory. An isogeometric Kirchhoff–Love shell formulation was first presented in [4] and was later extended to account for local refinement [15–17], material nonlinearities [5, 18, 19], fracture and damage [20–23] and gradient elasticity [24]. While IGA on a single NURBS patch is generally simple and straightforward, there are two aspects which make it more complicated for complex CAD models, namely trimming and patch coupling.

Trimming refers to “cutting off” parts of a surface along a trimming curve, and it is an essential technology for modeling com-

plex geometries with simple tensor-product NURBS patches. For isogeometric analysis on trimmed patches, special integration rules are necessary for trimmed elements, i.e. elements which are intersected by the trimming curve. Several approaches to perform IGA on trimmed geometries have been developed [25–31], where many of them share similarities to immersed methods such as the finite cell method [32] or CutFEM [33].

Patch coupling is needed whenever a model consists of more than one NURBS patch. The difficulty comes from the fact that in complex CAD models patches are typically non-conforming, meaning that they do not share the same parametrization along a common boundary, or even non-watertight, meaning that there are small gaps and overlaps between the two patches to be coupled. In the case of Kirchhoff–Love shell analysis, an additional complication arises from the C^1 continuity constraint, which has to be imposed across patch boundaries. While the term C^1 continuity actually applies only to smooth patch connections, we speak more generally of *rotational continuity*, meaning that the patches to be coupled must describe the same rotation around the common boundary, or, in other words, that the angle between patches must remain constant. A lot of research has been devoted to patch coupling for isogeometric Kirchhoff–Love shell analysis, and many different methods have been proposed, including strong coupling [4, 34–36], penalty methods [18, 28, 37, 38] and Nitsche’s method [16, 31, 39]. In [1], a simple and versatile penalty formulation has been presented for enforcing displacement and rotational continuity between patches, as well as displacement and rotational boundary conditions, with a single, dimensionless, penalty parameter. This formulation has been applied to the modeling and

Received: 30 December 2021; Accepted: 9 February 2022

© The Author(s) 2022. Published by Oxford University Press on behalf of Society of Theoretical and Applied Mechanics of the Republic of China, Taiwan. This is an Open Access article distributed under the terms of the Creative Commons Attribution License (<https://creativecommons.org/licenses/by/4.0/>), which permits unrestricted reuse, distribution, and reproduction in any medium, provided the original work is properly cited.

optimization of wind turbine blades in [40], and has been extended for phase-field fracture simulations of multipatch shell structures in [41, 42]. In [43], the formulation of [1] was rewritten in a Hellinger–Reissner form, obtaining a penalty coupling formulation with increased robustness, while [44] developed a super-penalty approach based on [1] with optimal convergence rates.

While the coupling formulation presented in [1] is generally applicable to arbitrary patch connections, only the simple case of coupling along untrimmed patch boundaries has been considered in the original contribution. In the present contribution, we extend this approach to the more general case of arbitrary coupling curves. A focus is set on trimming curves due to their importance in CAD modeling, but the formulation is not limited to trimming curves. Other relevant cases could be coupling along intersection curves of patches or imposing boundary conditions along arbitrary curves within a patch. For all these cases, we assume that the penalty constraint has to be enforced along an independent curve, which may be described either in the physical space or in the parametric space of one of the patches. For both cases, we derive detailed formulations ready for implementation. Finally, the presented method is validated on a set of numerical examples. First, we consider a well-known shell benchmark example with a simple geometry, which allows for validation against results obtained on an untrimmed single NURBS patch. Secondly, we consider a complex geometry, obtained from a CAD software using projection, trimming and sweeping operations, demonstrating the versatility and applicability of the method. For both examples, linear and geometrically nonlinear analyses are performed and validated against reference results, confirming the accuracy of the method.

2. KIRCHHOFF–LOVE SHELL FORMULATION AND PENALTY PATCH COUPLING

In this section, the equations of the shell formulation and the patch coupling formulation are briefly reviewed, where everything is formulated in terms of geometric properties of the shell's midsurface in the deformed and undeformed configurations. A point on the midsurface is described by the position vector $\mathbf{r}(\xi^1, \xi^2)$ in the deformed configuration and by $\hat{\mathbf{r}}(\hat{\xi}^1, \hat{\xi}^2)$ in the undeformed configuration, with $\mathbf{r} = \hat{\mathbf{r}} + \mathbf{u}$, where \mathbf{u} is the displacement vector. ξ^1 and ξ^2 are curvilinear surface coordinates, and the notation (\cdot) generally refers to the undeformed configuration. Where suitable, we employ index notation with Greek indices ranging from 1 to 2, and partial derivatives are indicated by a comma. The covariant tangent vectors of the surface are obtained as

$$\mathbf{a}_\alpha = \frac{\partial \mathbf{r}}{\partial \xi^\alpha} = \mathbf{r}_{,\alpha}. \quad (1)$$

The thickness direction of the shell is defined by the unit normal vector

$$\mathbf{a}_3 = \frac{\mathbf{a}_1 \times \mathbf{a}_2}{\|\mathbf{a}_1 \times \mathbf{a}_2\|}, \quad (2)$$

and the thickness coordinate ξ_3 , with $-t/2 \geq \xi_3 \geq t/2$ and t as the shell thickness.

With the covariant base vectors, the strain variables $\boldsymbol{\varepsilon}$ and $\boldsymbol{\kappa}$ representing membrane strains and curvature changes, respectively, are defined as

$$\varepsilon_{\alpha\beta} = \frac{1}{2}(\mathbf{a}_\alpha \cdot \mathbf{a}_\beta - \hat{\mathbf{a}}_\alpha \cdot \hat{\mathbf{a}}_\beta), \quad (3)$$

$$\kappa_{\alpha\beta} = \hat{\mathbf{a}}_{\alpha,\beta} \cdot \hat{\mathbf{a}}_3 - \mathbf{a}_{\alpha,\beta} \cdot \mathbf{a}_3. \quad (4)$$

Assuming linear elastic material, described by the material tensor \mathbb{C} , membrane forces \mathbf{n} and moments \mathbf{m} are obtained as

$$\mathbf{n} = t \mathbb{C} \boldsymbol{\varepsilon}, \quad (5)$$

$$\mathbf{m} = \frac{t^3}{12} \mathbb{C} \boldsymbol{\kappa}. \quad (6)$$

This formulation can be readily extended to nonlinear constitutive models as shown in detail in [5, 19]. The variational problem is expressed by the virtual work principle, where virtual quantities are denoted by δ and the internal virtual work of the Kirchhoff–Love shell is obtained as

$$\delta W^{\text{int}} = \int_S (\delta \boldsymbol{\varepsilon} : \mathbf{n} + \delta \boldsymbol{\kappa} : \mathbf{m}) dS. \quad (7)$$

The integral in Eq. (7) can be computed in different ways, e.g. standard element-wise integration [2] or patch-wise integration [45] for untrimmed NURBS patches. For trimmed elements, special integration rules have to be adopted, and different solutions have been proposed in the literature, including the NURBS-enhanced triangles method [25, 26], the adaptive Gaussian integration procedure [28] and the blending function method [46]. In our implementation, we adopt the blending function approach, but we highlight that the formulation for patch coupling along trimming lines as presented in the following is independent of the integration scheme for trimmed elements.

If the shell structure is modeled by several NURBS patches, continuity constraints have to be imposed on their interfaces. For Kirchhoff–Love shells, these include displacement continuity and rotational continuity. According to [1], this can be obtained by augmenting the virtual work expression by two penalty terms W^{pd} and W^{pr} , enforcing displacement and rotational continuity, respectively. Considering two patches \mathcal{S}^A and \mathcal{S}^B that share an interface curve \mathcal{L} , the penalty terms are defined as

$$\delta W^{\text{pd}} = \int_{\mathcal{L}} \alpha_d (\mathbf{u}^A - \mathbf{u}^B) \cdot (\delta \mathbf{u}^A - \delta \mathbf{u}^B) d\mathcal{L}, \quad (8)$$

$$\begin{aligned} \delta W^{\text{pr}} = & \int_{\mathcal{L}} \alpha_r ((\mathbf{a}_3^A \cdot \mathbf{a}_3^B - \hat{\mathbf{a}}_3^A \cdot \hat{\mathbf{a}}_3^B) (\delta \mathbf{a}_3^A \cdot \mathbf{a}_3^B + \mathbf{a}_3^A \cdot \delta \mathbf{a}_3^B) \\ & + (\mathbf{a}_n^A \cdot \mathbf{a}_3^B - \hat{\mathbf{a}}_n^A \cdot \hat{\mathbf{a}}_3^B) (\delta \mathbf{a}_n^A \cdot \mathbf{a}_3^B + \mathbf{a}_n^A \cdot \delta \mathbf{a}_3^B)) d\mathcal{L}, \end{aligned} \quad (9)$$

where the penalty parameters α_d and α_r are controlled by a single dimensionless penalty parameter α as

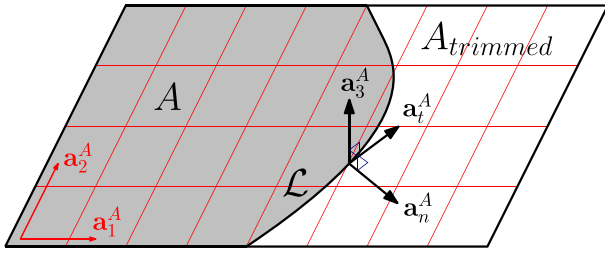


Figure 1 Patch S^A trimmed by curve \mathcal{L} , which is also the coupling line, with the vectors \mathbf{a}_t^A , \mathbf{a}_n^A and \mathbf{a}_3^A . The covariant base vectors \mathbf{a}_1^A and \mathbf{a}_2^A , and the mesh lines are indicated in red.

$$\alpha_d = \alpha \frac{Et}{h(1-\nu^2)}, \quad (10)$$

$$\alpha_r = \alpha \frac{Et^3}{12h(1-\nu^2)}, \quad (11)$$

with E as Young's modulus, ν as Poisson's ratio and t as thickness of the shells, while h is an average element length in \mathcal{L} . If material and/or thickness parameters vary between the patches to be connected, one may simply use their average values for Eqs. (10) and (11). For further details, reference is made to [1], where $\alpha = 10^3$ has been found as a problem-independent recommended value.

The vector \mathbf{a}_n denotes a unit vector lying in the tangent plane of the patch and perpendicular to \mathcal{L} . It can be computed from the out-of-plane normal vector \mathbf{a}_3 and the unit tangent vector \mathbf{a}_t of \mathcal{L} as

$$\mathbf{a}_n = \mathbf{a}_t \times \mathbf{a}_3, \quad (12)$$

$$\mathbf{a}_t = \frac{\tilde{\mathbf{a}}_t}{\|\tilde{\mathbf{a}}_t\|}, \quad (13)$$

where $\tilde{\mathbf{a}}_t$ is the covariant tangent vector of the coupling curve \mathcal{L} , see Fig. 1.

The augmented virtual work expression then reads as

$$\delta W = \delta W^{\text{int}} + \delta W^{\text{pd}} + \delta W^{\text{pr}} - \delta W^{\text{ext}} = 0, \quad (14)$$

where δW^{ext} is the external virtual work. The variational formulation (14) provides the basis for the solution via a numerical discretization scheme. Since δW^{int} contains second derivatives of the solution (cf. Eq. (4)), C^1 -continuous shape functions are needed for discretization, which can be provided by NURBS-based IGA within each NURBS patch, while continuity across patch interfaces is enforced by the penalty terms δW^{pd} and δW^{pr} . We note that this formulation requires only displacement degrees of freedom, but no rotational degrees of freedom. This also motivates the specific formulation of δW^{pr} (9), which does not employ rotations, only normal vectors and their scalar products.

After discretization, Eq. (14) is linearized and solved via a Newton–Raphson scheme

$$\frac{\partial^2 \delta W}{\partial u_r \partial u_s} \Delta u_s = -\frac{\partial \delta W}{\partial u_r}, \quad (15)$$

where u_r and u_s represent the displacement degrees of freedom, i.e. control point displacements. The first derivatives of δW represent the components of the residual force vector \mathbf{R} , while the

second derivatives correspond to the tangent stiffness matrix \mathbf{K} . Accordingly, Eq. (15) can be expressed in the classical format as

$$\mathbf{K} \Delta \mathbf{u} = -\mathbf{R}. \quad (16)$$

The variations of δW^{int} and δW^{ext} with respect to u_r and u_s can be found in detail in [4, 5], those of the penalty terms δW^{pd} and δW^{pr} are derived in [1]. While the variations of δW^{pd} are standard, those of δW^{pr} are more specific and are repeated here for the sake of clarity in the following discussion:

$$\begin{aligned} \frac{\partial W^{\text{pr}}}{\partial u_r} = \int_{\mathcal{L}} \alpha_r & \left((\mathbf{a}_3^A \cdot \mathbf{a}_3^B - \hat{\mathbf{a}}_3^A \cdot \hat{\mathbf{a}}_3^B) (\mathbf{a}_{3,r}^A \cdot \mathbf{a}_3^B + \mathbf{a}_3^A \cdot \mathbf{a}_{3,r}^B) \right. \\ & \left. + (\mathbf{a}_n^A \cdot \mathbf{a}_3^B - \hat{\mathbf{a}}_n^A \cdot \hat{\mathbf{a}}_3^B) (\mathbf{a}_{n,r}^A \cdot \mathbf{a}_3^B + \mathbf{a}_n^A \cdot \mathbf{a}_{3,r}^B) \right) d\mathcal{L}, \end{aligned} \quad (17)$$

$$\begin{aligned} \frac{\partial W^{\text{pr}}}{\partial u_r \partial u_s} = \int_{\mathcal{L}} \alpha_r & \left((\mathbf{a}_3^A \cdot \mathbf{a}_3^B - \hat{\mathbf{a}}_3^A \cdot \hat{\mathbf{a}}_3^B) (\mathbf{a}_{3,rs}^A \cdot \mathbf{a}_3^B \right. \\ & + \mathbf{a}_{3,r}^A \cdot \mathbf{a}_{3,s}^B + \mathbf{a}_{3,s}^A \cdot \mathbf{a}_{3,r}^B + \mathbf{a}_3^A \cdot \mathbf{a}_{3,rs}^B) \\ & + (\mathbf{a}_{3,s}^A \cdot \mathbf{a}_3^B + \mathbf{a}_3^A \cdot \mathbf{a}_{3,s}^B) (\mathbf{a}_{3,r}^A \cdot \mathbf{a}_3^B + \mathbf{a}_3^A \cdot \mathbf{a}_{3,r}^B) \\ & + (\mathbf{a}_n^A \cdot \mathbf{a}_3^B - \hat{\mathbf{a}}_n^A \cdot \hat{\mathbf{a}}_3^B) (\mathbf{a}_{n,rs}^A \cdot \mathbf{a}_3^B + \mathbf{a}_{n,r}^A \cdot \mathbf{a}_{3,s}^B \\ & + \mathbf{a}_{n,s}^A \cdot \mathbf{a}_{3,r}^B + \mathbf{a}_n^A \cdot \mathbf{a}_{3,rs}^B) \\ & \left. + (\mathbf{a}_{n,s}^A \cdot \mathbf{a}_3^B + \mathbf{a}_n^A \cdot \mathbf{a}_{3,s}^B) (\mathbf{a}_{n,r}^A \cdot \mathbf{a}_3^B + \mathbf{a}_n^A \cdot \mathbf{a}_{3,r}^B) \right) d\mathcal{L}. \end{aligned} \quad (18)$$

We note that the penalty terms for rotational continuity require only the out-of-plane normal vectors \mathbf{a}_3 of both patches and the in-plane normal vector \mathbf{a}_n of one of the patches, as well as their variations with respect to u_r and u_s . It also should be noted that \mathbf{a}_3 and its variations are part of the structural stiffness matrix derived from δW^{int} (see Eqs. (4) and (7)), and can be found in detail in [5]. The variations of \mathbf{a}_n are obtained by applying the chain rule to Eq. (12) as

$$\mathbf{a}_{n,r} = \mathbf{a}_{t,r} \times \mathbf{a}_3 + \mathbf{a}_t \times \mathbf{a}_{3,r}, \quad (19)$$

$$\mathbf{a}_{n,rs} = \mathbf{a}_{t,rs} \times \mathbf{a}_3 + \mathbf{a}_{t,r} \times \mathbf{a}_{3,s} + \mathbf{a}_{t,s} \times \mathbf{a}_{3,r} + \mathbf{a}_t \times \mathbf{a}_{3,rs}, \quad (20)$$

where the variations of \mathbf{a}_t are obtained from Eq. (13) as

$$\mathbf{a}_{t,r} = \frac{1}{\|\tilde{\mathbf{a}}_t\|} (\tilde{\mathbf{a}}_{t,r} - (\mathbf{a}_t \cdot \tilde{\mathbf{a}}_{t,r}) \mathbf{a}_t), \quad (21)$$

$$\begin{aligned} \mathbf{a}_{t,rs} = & -\frac{1}{\|\tilde{\mathbf{a}}_t\|} (\mathbf{a}_{t,s} \cdot \tilde{\mathbf{a}}_{t,r}) \mathbf{a}_t + \frac{1}{\|\tilde{\mathbf{a}}_t\|^2} (2 (\mathbf{a}_t \cdot \tilde{\mathbf{a}}_{t,r}) (\mathbf{a}_t \cdot \tilde{\mathbf{a}}_{t,s}) \mathbf{a}_t \\ & - (\mathbf{a}_t \cdot \tilde{\mathbf{a}}_{t,s}) \tilde{\mathbf{a}}_{t,r} - (\mathbf{a}_t \cdot \tilde{\mathbf{a}}_{t,r}) \tilde{\mathbf{a}}_{t,s}). \end{aligned} \quad (22)$$

With Eqs. (19)–(22) we have all terms needed for the computation of rotational penalty terms, provided that $\tilde{\mathbf{a}}_t$ and its variations with respect to the degrees of freedom of the patch S^A are accessible. If the coupling curve \mathcal{L} corresponds to an edge of one of the patches (which can then be assigned as S^A), $\tilde{\mathbf{a}}_t$ corresponds to either \mathbf{a}_1 or \mathbf{a}_2 of that patch, depending on the edge.

Accordingly, the variations $\tilde{\mathbf{a}}_{t,r}$ and $\tilde{\mathbf{a}}_{t,rs}$ are simply given by the variations of \mathbf{a}_1 or \mathbf{a}_2 , which, again, are part of the structural stiffness matrix derived from δW^{int} (see Eqs. (3) and (7)), and can be found in detail in [5]. Furthermore, the integration domain of Eqs. (17) and (18) and its parametrization are then given by the corresponding patch edge [1].

However, in many cases, coupling is not performed simply along patch boundaries, but along trimming curves. Other possible scenarios could be the coupling of two patches along their intersection curve or the imposition of Dirichlet boundary conditions along arbitrary curves within a patch via the penalty formulation. The formulation presented in the next section can be applied to all these cases.

3. COUPLING ALONG ARBITRARY LINES

In this section, the penalty formulation for rotational continuity (17)–(22), initially proposed in [1], is extended to the application on arbitrary coupling curves. In general, such coupling curves may be described as NURBS curves either in the physical space or in the parametric spaces of the patches involved. In the following, both cases are presented in detail.

3.1 Coupling curve in the physical space

We assume that the coupling curve \mathcal{L} is described as a spatial curve $\mathbf{c}(\eta)$ in the physical space with η as the curve parameter. The tangent $\tilde{\mathbf{a}}_t$ can be obtained as the curve's derivative with respect to η :

$$\tilde{\mathbf{a}}_t = \frac{\partial \mathbf{c}}{\partial \eta}, \quad (23)$$

and integrals along this curve can be generally computed as

$$\int_{\mathcal{L}} d\mathcal{L} = \int_{\eta=0}^{\eta=1} \|\tilde{\mathbf{a}}_t\| d\eta, \quad (24)$$

where, without loss of generality, $0 \leq \eta \leq 1$ is assumed.

For the penalty terms (17) and (18), $\tilde{\mathbf{a}}_t$ needs to be projected onto \mathcal{S}^A such that the variations $\tilde{\mathbf{a}}_{t,r}$ and $\tilde{\mathbf{a}}_{t,rs}$ with respect to the degrees of freedom of \mathcal{S}^A can be computed. This projection can be obtained as follows:

$$\tilde{\mathbf{a}}_t^A = c_1 \mathbf{a}_1^A + c_2 \mathbf{a}_2^A = (\mathbf{c} \cdot \mathbf{a}_1^A) \mathbf{a}_1^A + (\mathbf{c} \cdot \mathbf{a}_2^A) \mathbf{a}_2^A. \quad (25)$$

Since the location of the coupling curve within the parametric space of \mathcal{S}^A does not change during deformation, the coefficients c_1 and c_2 can equally be computed in the undeformed configuration

$$\tilde{\mathbf{a}}_t^A = c_1 \mathbf{a}_1^A + c_2 \mathbf{a}_2^A = (\dot{\mathbf{c}} \cdot \dot{\mathbf{a}}_1^A) \mathbf{a}_1^A + (\dot{\mathbf{c}} \cdot \dot{\mathbf{a}}_2^A) \mathbf{a}_2^A. \quad (26)$$

In Eq. (26), $\tilde{\mathbf{a}}_t^A$ depends only linearly on \mathbf{u} , and the variations $\tilde{\mathbf{a}}_{t,r}^A$, $\tilde{\mathbf{a}}_{t,rs}^A$ are simply obtained as

$$\tilde{\mathbf{a}}_{t,r}^A = (\dot{\mathbf{c}} \cdot \dot{\mathbf{a}}_1^A) \mathbf{a}_{1,r}^A + (\dot{\mathbf{c}} \cdot \dot{\mathbf{a}}_2^A) \mathbf{a}_{2,r}^A, \quad (27)$$

$$\tilde{\mathbf{a}}_{t,rs}^A = (\dot{\mathbf{c}} \cdot \dot{\mathbf{a}}_1^A) \mathbf{a}_{1,rs}^A + (\dot{\mathbf{c}} \cdot \dot{\mathbf{a}}_2^A) \mathbf{a}_{2,rs}^A, \quad (28)$$

where the variations of \mathbf{a}_1 and \mathbf{a}_2 are already contained in the structural stiffness matrix and are detailed in [5].

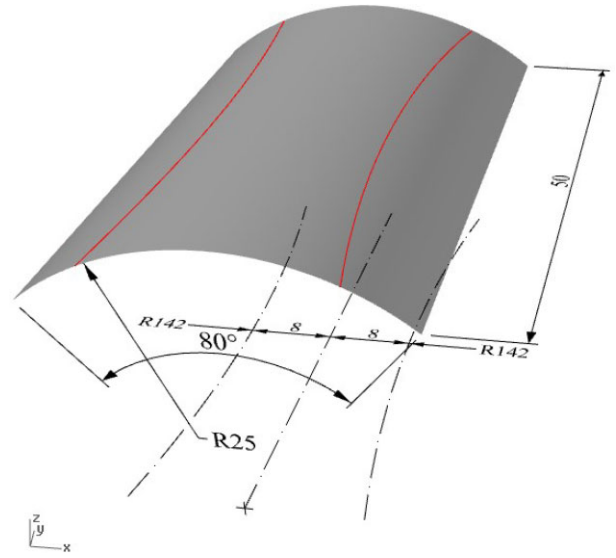


Figure 2 Scordelis–Lo roof: geometry, dimensions in mm and division into trimmed patches by the trimming curves highlighted in red. The trimming curves are a projection of the dash-dotted arcs from the x – y plane onto the surface. The radius of the arcs is 142 mm, and their distance from the y – z symmetry plane of the geometry is 8 mm.

3.2 Coupling curve in the parametric space

Alternatively, the coupling curve may be directly described as planar curve in the parametric space of one of the patches. In the following, this patch is indicated as \mathcal{S}^A , and the coupling curve as \mathbf{c}^A :

$$\mathbf{c}^A(\eta) = \begin{bmatrix} c_1^A(\eta) \\ c_2^A(\eta) \end{bmatrix}. \quad (29)$$

The tangent $\tilde{\mathbf{a}}_t^A$ (in the physical space) and its variations are then simply obtained as

$$\tilde{\mathbf{a}}_t^A = \frac{\partial c_1^A}{\partial \eta} \mathbf{a}_1^A + \frac{\partial c_2^A}{\partial \eta} \mathbf{a}_2^A, \quad (30)$$

$$\tilde{\mathbf{a}}_{t,r}^A = \frac{\partial c_1^A}{\partial \eta} \mathbf{a}_{1,r}^A + \frac{\partial c_2^A}{\partial \eta} \mathbf{a}_{2,r}^A, \quad (31)$$

$$\tilde{\mathbf{a}}_{t,rs}^A = \frac{\partial c_1^A}{\partial \eta} \mathbf{a}_{1,rs}^A + \frac{\partial c_2^A}{\partial \eta} \mathbf{a}_{2,rs}^A, \quad (32)$$

and integration is performed as

$$\int_{\mathcal{L}} d\mathcal{L} = \int_{\eta=0}^{\eta=1} \|\tilde{\mathbf{a}}_t^A\| d\eta. \quad (33)$$

3.3 Point inversion and point projection

For the evaluation of the integral terms in Eqs. (17) and (18), the coordinates of the integration points, defined in the parametric space of the coupling curve, are needed in the parametric spaces of the patches. This is called point inversion. In complex CAD models, patch connections are often not watertight, which means that the corresponding trimming curves on both patches do not exactly coincide. In such cases, the integration points need to be projected onto the patches. (If the coupling curve is defined in the parametric space of \mathcal{S}^A , projection is needed only onto \mathcal{S}^B .) In our implementation, we employ the algorithm from

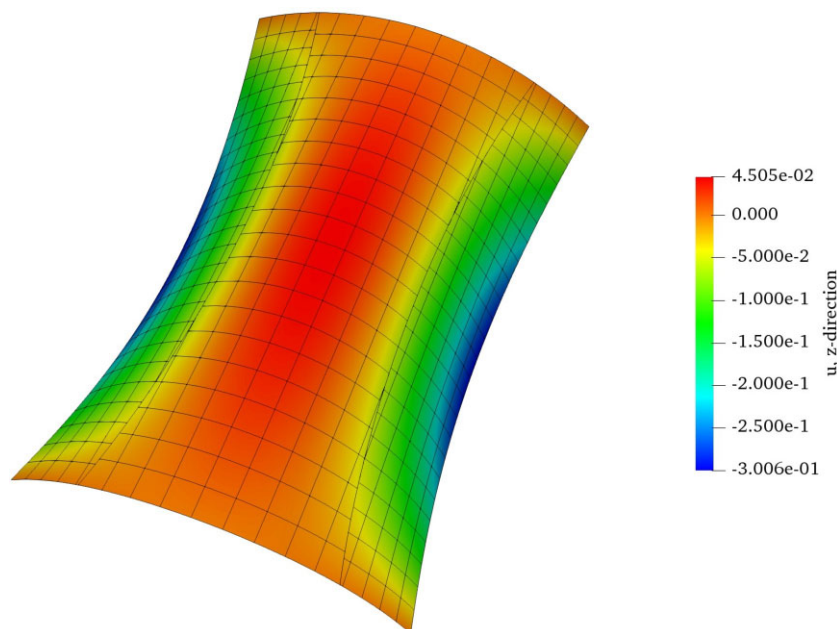


Figure 3 Linear analysis of the trimmed model of the Scordelis–Lo roof. The displayed mesh comprises 20×25 for the side patches and 15×20 elements for the central patch, before trimming. This mesh has 1831 total degrees of freedom for $p = 2$ and 2143 degrees of freedom for $p = 3$. The deformed structure is scaled by a factor of 15 for visualization purposes, and the color scheme indicates the displacement in z -direction.

[47], which is a simple and efficient method based on a Newton iteration, involving only position and tangent vectors of points on the curve and the patches. For the detailed algorithm, we refer to [47]. An interesting feature of this algorithm is that it works equally for point inversion and point projection. This is an important advantage, since in complex multipatch CAD models, it is not necessarily clear which patch connections are watertight and which are not. The penalty coupling formulation presented in the previous sections together with this algorithm for point inversion/projection allows for structural analysis on complex CAD models with arbitrary patch connections.

4. NUMERICAL EXAMPLES

The formulation presented in the previous sections is now tested on selected numerical examples. The first example is the well-known Scordelis–Lo roof problem. In this case, the geometry will be divided into three trimmed patches while a single patch IGA solution is used as a reference. The second example presents a more complex geometry consisting of two intersecting tubes. Here, we use the commercial FEA program *Abaqus* of *Dassault Systems* for computing a reference solution. All geometries are created in the CAD program *Rhinoceros* of *McNeel*. For both examples, we perform linear and geometrically nonlinear analysis, and in all simulations, the value $\alpha = 10^3$ for the penalty coefficient is used.

4.1 Scordelis–Lo roof

The Scordelis–Lo roof is one of the problems included in the shell obstacle course [48]. We divide the geometry into three patches as in [31], see Fig. 2. The red lines indicate the trimming curves, which are obtained as the projection of two circu-

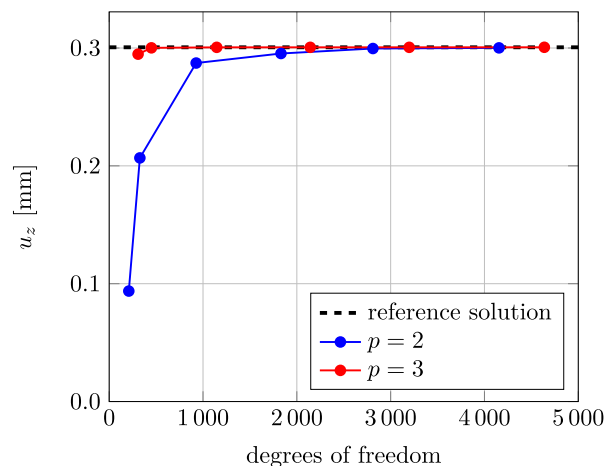


Figure 4 Linear analysis of the trimmed model of the Scordelis–Lo roof. Convergence of the vertical displacement u_z at the midpoint of the side edge for different mesh densities and degrees of the shape functions.

lar arches with radius 142 mm from the x – y plane onto the shell. At the curved edges, the displacements in x and z -direction are constrained, while the other two edges are left free. The penalty coupling is enforced along the trimming curves defined in the parametric space of the outer patches. A uniformly distributed load is imposed in the negative z -direction. Linear elastic material is considered, with Young's modulus $E = 4.32 \times 10^8$ N/mm² and Poisson's ratio $\nu = 0$. The shell thickness is $t = 0.25$ mm. We first perform geometrically linear analysis with the load equal to 90 N/mm², as usually considered in the literature. Figure 3 depicts the resulting deformed geometry with a color plot of the deformation in z -direction for one of the considered meshes, while

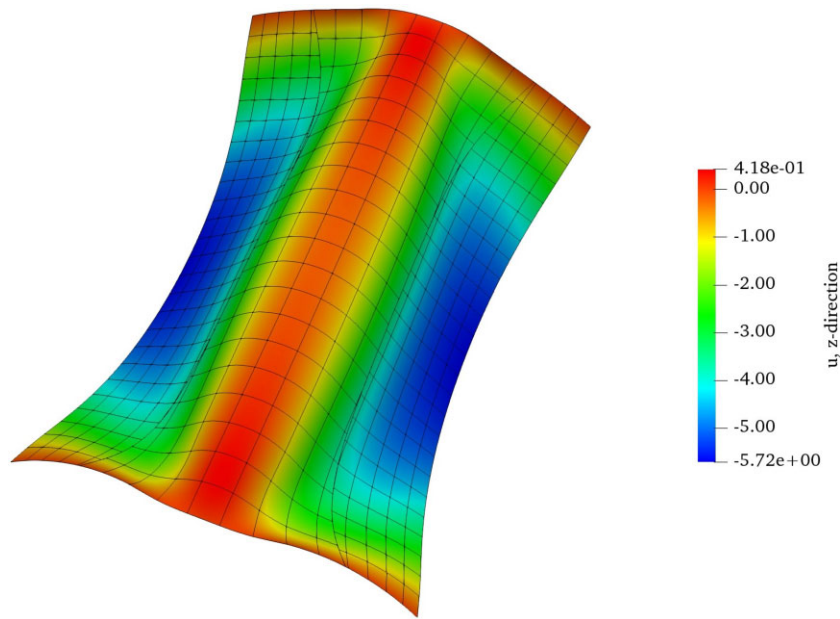


Figure 5 Result of the geometrically nonlinear analysis for the trimmed model of the Scordelis–Lo roof in terms of displacements in z -direction.

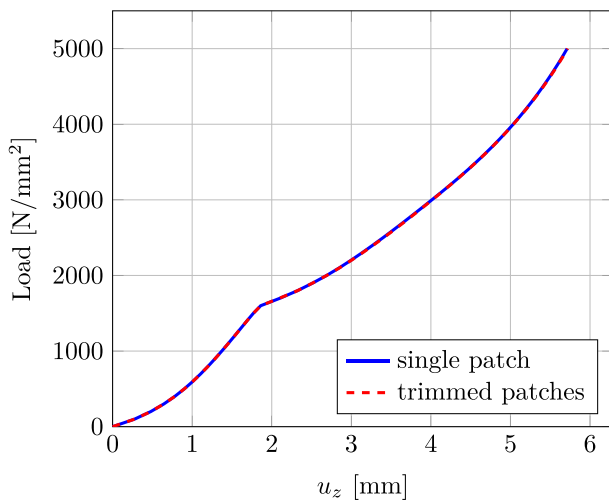


Figure 6 Load–displacement curves for the single patch and trimmed models of the geometrically nonlinear Scordelis–Lo roof problem.

Fig. 4 shows the convergence of the solution, in terms of z displacement at the midpoint of the side edge, for degrees $p = 2$ and $p = 3$. The converged reference value is taken as $u_z = 0.3006$ mm from the result of the single patch analysis [4].

To test the proposed formulation in the large displacement framework, we increase the load up to 5000 N/mm² and perform geometrical nonlinear analysis. The results of a single patch model with a mesh constituted by 15×20 elements and of the trimmed model having a mesh as the one depicted in Fig. 3 are compared (the degree of the shape functions is $p = 3$ in both cases). Figure 5 shows the final deformed geometry of the trimmed model, while Fig. 6 depicts the load–displacement curves (with u_z evaluated again at the midpoint of the side edge) for the trimmed and untrimmed models, showing an excellent agreement.

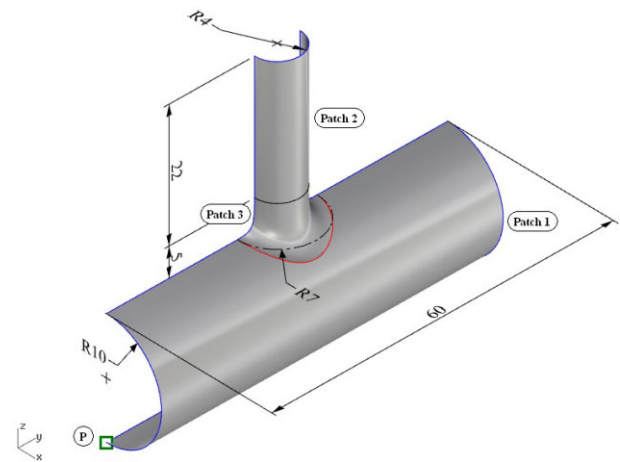


Figure 7 Intersecting tubes problem: geometry, dimensions in mm and division in patches by the black and by the red curve, which is also a trimming line. Edges along which symmetry conditions are imposed are highlighted in blue. The reference point P for the comparison of the displacements in the linear model is highlighted in green.

4.2 Intersecting tubes

This example features a complex CAD geometry constituted by two intersecting cylinders connected by a fillet. It is inspired by a similar example proposed in [31], but in our case a different geometry of the fillet is considered. Figure 7 shows the geometry, the dimensions and the division into patches. Due to symmetry, only half of the geometry is modeled. The model consists of three patches, two for the cylinders (the larger one will be referred to as patch 1 and the smaller one as patch 2) and one for the fillet (referred to as patch 3). Patch 1 is trimmed by the trimming curve indicated in red in Fig. 7. This curve is obtained as the projection of the circle indicated by a dash–dotted line from the x – y plane onto the cylinder. The fillet is created by a sweep

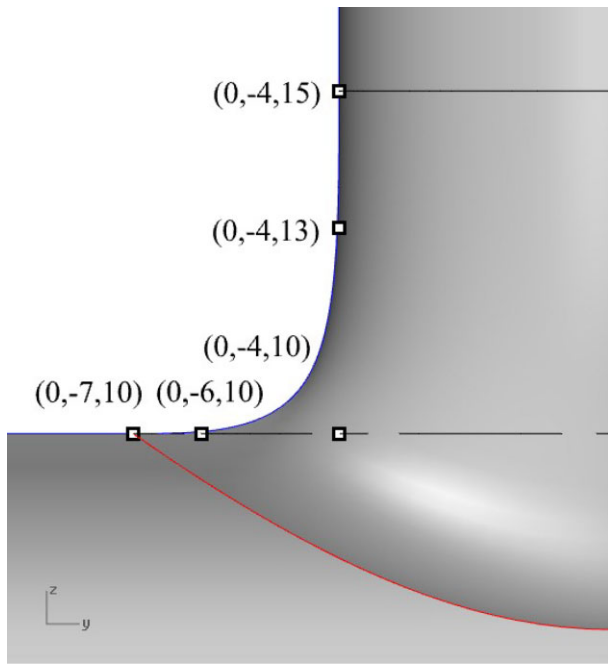


Figure 8 Details of one of the two rail curves along which the sweep operation for generating patch 3 is performed. Control points coordinates refer to the coordinate system with the origin in the point corresponding to the intersection of the axes of the two cylinders, control weights are all unitary, the polynomial degree is $p = 3$ and the knot vector is $[0, 0, 0, 0, 0.5, 1, 1, 1, 1]$.

operation between this trimming curve and the lower boundary of patch 2. The rails for the sweep operation are two curves lying in the y - z plane. The first one is depicted with a detailed de-

scription in Fig. 8, and the second one is defined symmetrically to it with respect to the x - z plane. Patch 1 and patch 3 are coupled along the trimming curve defined in the parametric space of patch 1, while patch 2 and patch 3 are coupled along the lower edge of patch 2. On the free boundaries, indicated by blue lines in Fig. 7, symmetry conditions are applied, which are imposed via the same penalty formulation [1]. The polynomial degree is $p = 4$ for all the three patches, and meshes counting 44×66 , 36×44 and 32×23 control points are used for patches 1, 2 and 3, respectively. The shell thickness is $t = 0.2$ mm, and a linear elastic material with Young's modulus $E = 3 \times 10^6$ N/mm² and Poisson's ratio $\nu = 0.3$ is considered.

First, we perform linear analysis for a load corresponding to internal pressure of 1 MPa on all patches. Figure 9 displays the deformed geometry with a color scheme indicating the absolute displacement magnitude, together with the undeformed configuration for reference. The displacement in z -direction at point P depicted in Fig. 7 is equal to $u_z = 1.477 \times 10^{-3}$ mm. For validation, this result is compared with one obtained by the commercial finite-element software *Abaqus* using a general purpose quadratic shell element with reduced integration (S8R). The *Abaqus* solution for point P is $u_z = 1.501 \times 10^{-3}$ mm, showing a good agreement with the solution obtained applying the proposed formulation, also for this challenging geometry.

As for the Scordelis-Lo roof example, we further test the formulation in the geometrically nonlinear setting. In order to induce more bending deformation, we change the loading and boundary conditions. Instead of internal pressure, we impose a displacement of 3.5 mm in the positive y -direction at the top edge of patch 2, removing the symmetry condition on this edge and without imposing any other constraint. In order to prevent

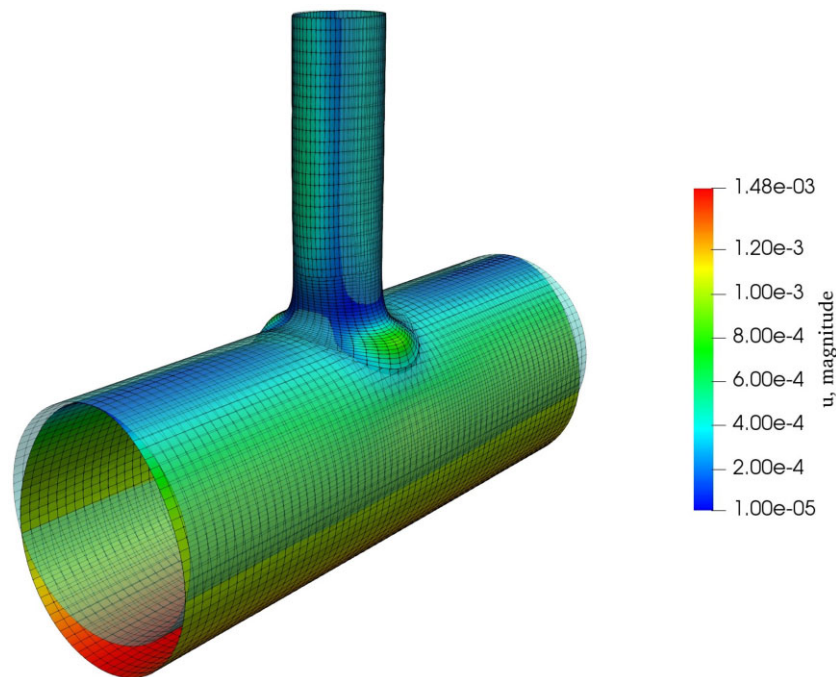


Figure 9 Linear analysis for the intersecting tubes problem with internal pressure. The full structure is shown for visualization purposes. The deformation is scaled by a factor of 2×10^3 , the color scheme indicates the absolute displacement magnitude, while the shaded surface represents the undeformed geometry.

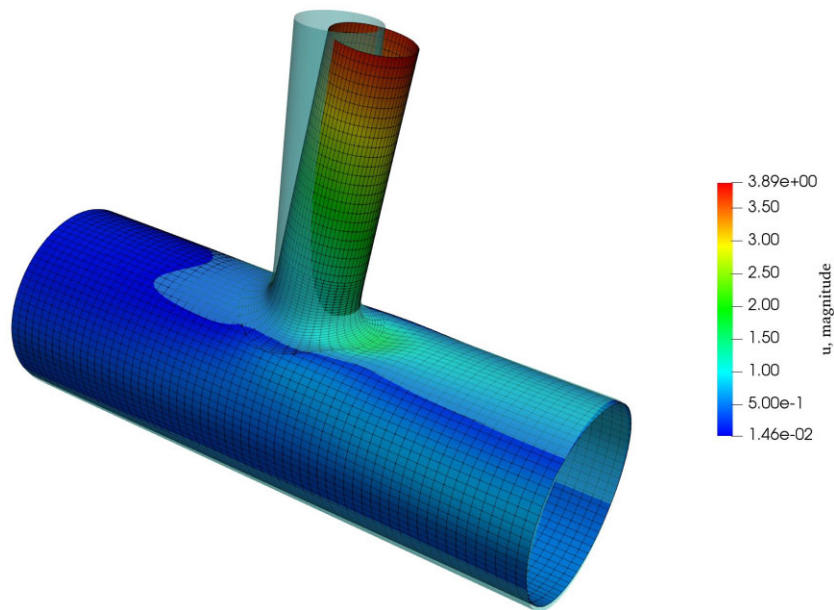


Figure 10 Geometrically nonlinear analysis for the intersecting tubes problem with imposed displacement. The full structure is shown for visualization purposes. The color scheme indicates the absolute displacement magnitude, while the shaded surface represents the undeformed geometry.

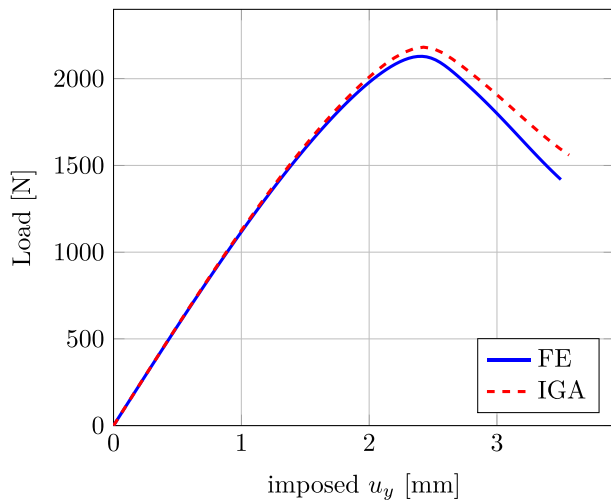


Figure 11 Load–displacement curves for the finite element and isogeometric models of the geometrically nonlinear example of the intersecting tubes.

rigid body motions, a point support in z -direction is applied at point P. Figure 10 displays the undeformed and deformed configurations with the magnitude of the displacements, while Fig. 11 depicts the corresponding load–displacement curves, together with the finite-element solution obtained from *Abaqus* for comparison. Also in this case, a good match can be observed. The load–displacement curves also show the highly nonlinear behavior of the structure, although deformations are still quite moderate, with a critical point corresponding to local buckling.

5. CONCLUSION

In this paper, we have presented a penalty-based patch coupling method allowing for isogeometric Kirchhoff–Love shell analysis on trimmed multipatch CAD models. The method is based on the penalty formulation presented in [1], which is extended to the application along arbitrary curves. While a focus is on trimming curves due to their relevance in CAD modeling, the formulation can be applied to any arbitrary curve, which may be defined either in the physical space or in the patch’s parametric space. For both cases, the detailed formulations have been presented in a ready-for-implementation form. We have tested the method on two numerical examples of different geometric complexity under linear and geometrically nonlinear analysis, demonstrating the accuracy and applicability of the proposed approach.

ACKNOWLEDGEMENTS

This work has received funding from the European Research Council (ERC) under the European Union’s Horizon 2020 research and innovation program (grant agreement No 864482).

REFERENCES

1. Herrema AJ, Johnson EL, Proserpio D, Wu MCH, Kiendl J, Hsu MC. Penalty coupling of non-matching isogeometric Kirchhoff–Love shell patches with application to composite wind turbine blades. *Computer Methods in Applied Mechanics and Engineering* 2019; **346**:810–840.
2. Hughes TJ, Cottrell JA, Bazilevs Y. Isogeometric analysis: CAD, finite elements, NURBS, exact geometry and mesh refinement. *Computer Methods in Applied Mechanics and Engineering* 2005; **194**(39):4135–4195.
3. Cottrell JA, Hughes TJ, Bazilevs Y. *Isogeometric Analysis: Toward Integration of CAD and FEA*. New York: Wiley, 2009.

4. Kiendl J, Bletzinger KU, Linhard J, Wüchner R. Isogeometric shell analysis with Kirchhoff–Love elements. *Computer Methods in Applied Mechanics and Engineering* 2009;**198**(49):3902–3914.
5. Kiendl J, Hsu MC, Wu MCH, Reali A. Isogeometric Kirchhoff–Love shell formulations for general hyperelastic materials. *Computer Methods in Applied Mechanics and Engineering* 2015;**291**:280–303.
6. Benson DJ, Bazilevs Y, Hsu MC, Hughes TJR. Isogeometric shell analysis: the Reissner–Mindlin shell. *Computer Methods in Applied Mechanics and Engineering* 2010;**199**(5):276–289.
7. Benson DJ, Bazilevs Y, Hsu MC, Hughes TJR. A large deformation, rotation-free, isogeometric shell. *Computer Methods in Applied Mechanics and Engineering* 2011;**200**(13):1367–1378.
8. Echter R, Oesterle B, Bischoff M. A hierarchic family of isogeometric shell finite elements. *Computer Methods in Applied Mechanics and Engineering* 2013;**254**:170–180.
9. Oesterle B, Sachse R, Ramm E, Bischoff M. Hierarchic isogeometric large rotation shell elements including linearized transverse shear parametrization. *Computer Methods in Applied Mechanics and Engineering* 2017;**321**:383–405.
10. Dornisch W, Klinkel S, Simeon B. Isogeometric Reissner–Mindlin shell analysis with exactly calculated director vectors. *Computer Methods in Applied Mechanics and Engineering* 2013;**253**:491–504.
11. Dornisch W, Vitucci G, Klinkel S. The weak substitution method—an application of the mortar method for patch coupling in NURBS-based isogeometric analysis. *International Journal for Numerical Methods in Engineering* 2015;**103**(3):205–234.
12. Caseiro JF, Valente RAF, Reali A, Kiendl J, Auricchio F, Alves de Sousa RJ. Assumed Natural Strain NURBS-based solid-shell element for the analysis of large deformation elasto-plastic thin-shell structures. *Computer Methods in Applied Mechanics and Engineering* 2015;**284**:861–880.
13. Kiendl J, Marino E, De Lorenzis L. Isogeometric collocation for the Reissner–Mindlin shell problem. *Computer Methods in Applied Mechanics and Engineering* 2017;**325**:645–665.
14. Alaydin MD, Benson DJ, Bazilevs Y. An updated lagrangian framework for isogeometric Kirchhoff–Love thin-shell analysis. *Computer Methods in Applied Mechanics and Engineering* 2021;**384**:113977.
15. Nguyen-Thanh N, Kiendl J, Nguyen-Xuan H, Wüchner R, Bletzinger KU, Bazilevs Y, Rabczuk T. Rotation free isogeometric thin shell analysis using PHT-splines. *Computer Methods in Applied Mechanics and Engineering* 2011;**200**(47):3410–3424.
16. Nguyen-Thanh N, Zhou K, Zhuang X, Areias P, Nguyen-Xuan H, Bazilevs Y, Rabczuk T. Isogeometric analysis of large-deformation thin shells using RHT-splines for multiple-patch coupling. *Computer Methods in Applied Mechanics and Engineering* 2017;**316**:1157–1178.
17. Zimmermann C, Sauer RA. Adaptive local surface refinement based on LRNURBS and its application to contact. *Computational Mechanics* 2017;**60**(6):1011–1031.
18. Duong TX, Roohbakhshan F, Sauer RA. A new rotation-free isogeometric thin shell formulation and a corresponding continuity constraint for patch boundaries. *Special Issue on Isogeometric Analysis: Progress and Challenges* 2017;**316**:43–83.
19. Ambati M, Kiendl J, De Lorenzis L. Isogeometric Kirchhoff–Love shell formulation for elasto-plasticity. *Computer Methods in Applied Mechanics and Engineering* 2018;**340**:320–339.
20. Nguyen-Thanh N, Valizadeh N, Nguyen MN, Nguyen-Xuan H, Zhuang X, Areias P, Zi G, Bazilevs Y, De Lorenzis L, Rabczuk T. An extended isogeometric thin shell analysis based on Kirchhoff–Love theory. *Computer Methods in Applied Mechanics and Engineering* 2015;**284**:265–291.
21. Kiendl J, Ambati M, De Lorenzis L, Gomez H, Reali A. Phase-field description of brittle fracture in plates and shells. *Computer Methods in Applied Mechanics and Engineering* 2016;**312**:374–394.
22. Pigazzini MS, Kamensky D, van Iersel DAP, Alaydin MD, Remmers JJC, Bazilevs Y. Gradient-enhanced damage modeling in Kirchhoff–Love shells: application to isogeometric analysis of composite laminates. *Computer Methods in Applied Mechanics and Engineering* 2019;**346**:152–179.
23. Behzadinasab M, Alaydin M, Trask N, Bazilevs Y. A general-purpose, inelastic, rotation-free Kirchhoff–Love shell formulation for peridynamics. *Computer Methods in Applied Mechanics and Engineering* 2022;**389**:114422.
24. Balabanov V, Kiendl J, Khakalo S, Niiranen J. Kirchhoff–Love shells within strain gradient elasticity: weak and strong formulations and an H3-conforming isogeometric implementation. *Computer Methods in Applied Mechanics and Engineering* 2019;**344**:837–857.
25. Kim HJ, Seo YD, Youn SK. Isogeometric analysis for trimmed CAD surfaces. *Computer Methods in Applied Mechanics and Engineering* 2009;**198**(37):2982–2995.
26. Kim HJ, Seo YD, Youn SK. Isogeometric analysis with trimming technique for problems of arbitrary complex topology. *Computer Methods in Applied Mechanics and Engineering* 2010;**199**(45):2796–2812.
27. Schmidt R, Wüchner R, Bletzinger KU. Isogeometric analysis of trimmed NURBS geometries. *Computer Methods in Applied Mechanics and Engineering* 2012;**241–244**:93–111.
28. Breitenberger M, Apostolatos A, Philipp B, Wüchner R, Bletzinger KU. Analysis in computer aided design: nonlinear isogeometric B-Rep analysis of shell structures. *Computer Methods in Applied Mechanics and Engineering* 2015;**284**:401–457.
29. Nagy AP, Benson DJ. On the numerical integration of trimmed isogeometric elements. *Computer Methods in Applied Mechanics and Engineering* 2015;**284**:165–185.
30. Beer G, Marussig B, Zechner J. A simple approach to the numerical simulation with trimmed CAD surfaces. *Computer Methods in Applied Mechanics and Engineering* 2015;**285**:776–790.
31. Guo Y, Ruess M, Schillinger D. A parameter-free variational coupling approach for trimmed isogeometric thin shells. *Computational Mechanics* 2017;**59**(4):693–715.
32. Rank E, Ruess M, Kollmannsberger S, Schillinger D, Düster A. Geometric modeling, isogeometric analysis and the finite cell method. *Computer Methods in Applied Mechanics and Engineering* 2012;**249–252**:104–115.
33. Burman E, Claus S, Hansbo P, Larson MG, Massing A. CutFEM: discretizing geometry and partial differential equations. *International Journal for Numerical Methods in Engineering* 2015;**104**:472–501.
34. Goyal A, Simeon B. On penalty-free formulations for multipatch isogeometric Kirchhoff–Love shells. *Mathematics and Computers in Simulation* 2017;**136**:78–103.
35. Coox L, Greco F, Atak O, Vandepitte D, Desmet W. A robust patch coupling method for NURBS-based isogeometric analysis of non-conforming multipatch surfaces. *Computer Methods in Applied Mechanics and Engineering* 2017;**316**:235–260.
36. Chan CL, Anitescu C, Rabczuk T. Isogeometric analysis with strong multipatch C1-coupling. *Computer Aided Geometric Design* 2018;**62**:294–310.
37. Kiendl J, Bazilevs Y, Hsu MC, Wüchner R, Bletzinger KU. The bending strip method for isogeometric analysis of Kirchhoff–Love shell structures comprised of multiple patches. *Computer Methods in Applied Mechanics and Engineering* 2010;**199**(37–40):2403–2416.
38. Lei Z, Gillot F, Jezequel L. A C0/G1 multiple patches connection method in isogeometric analysis. *Applied Mathematical Modelling* 2015;**39**(15):4405–4420.
39. Guo Y, Ruess M. Nitsche’s method for a coupling of isogeometric thin shells and blended shell structures. *Computer Methods in Applied Mechanics and Engineering* 2015;**284**:881–905.
40. Herrema AJ, Kiendl J, Hsu MC. A framework for isogeometric-analysis-based optimization of wind turbine blade structures. *Wind Energy* 2019;**22**(2):153–170.
41. Proserpio D, Ambati M, De Lorenzis L, Kiendl J. A framework for efficient isogeometric computations of phase-field brittle fracture in multipatch shell structures. *Computer Methods in Applied Mechanics and Engineering* 2020;**372**:113363.
42. Proserpio D, Ambati M, De Lorenzis L, Kiendl J. Phase-field simulation of ductile fracture in shell structures. *Computer Methods in Applied Mechanics and Engineering* 2021;**385**:114019.

43. Leonetti L, Liguori FS, Magisano D, Kiendl J, Reali A, Garcea G. A robust penalty coupling of non-matching isogeometric Kirchhoff–Love shell patches in large deformations. *Computer Methods in Applied Mechanics and Engineering* 2020;**371**: 113289.
44. Coradello L, Kiendl J, Buffa A. Coupling of non-conforming trimmed isogeometric Kirchhoff–Love shells via a projected superpenalty approach. *Computer Methods in Applied Mechanics and Engineering* 2021;**387**:114187.
45. Leonetti L, Magisano D, Madeo A, Garcea G, Kiendl J, Reali A. A simplified Kirchhoff–Love large deformation model for elastic shells and its effective isogeometric formulation. *Computer Methods in Applied Mechanics and Engineering* 2019;**354**:369–396.
46. Guo Y, Heller J, Hughes TJR, Ruess M, Schillinger D. Variationally consistent isogeometric analysis of trimmed thin shells at finite deformations, based on the STEP exchange format. *Computer Methods in Applied Mechanics and Engineering* 2018;**336**:39–79.
47. Piegl L, Tiller W. *The NURBS Book*. Berlin: Springer, 2012.
48. Belytschko T, Stolarski H, Liu WK, Carpenter N, Ong JSJ. Stress projection for membrane and shear locking in shell finite elements. *Computer Methods in Applied Mechanics and Engineering* 1985;**51**(1): 221–258.